

# An efficient general methodology to explore the high-temperature frontier in f-block molecular nanomagnets

*L. Escalera-Moreno,<sup>a</sup> Jose J. Baldovi,<sup>\*b</sup> E. Coronado<sup>a</sup>*

<sup>a</sup>Instituto de Ciencia Molecular (ICMol), Universidad de Valencia, c/ Catedrático José Beltrán 2, 46980, Paterna, Spain

<sup>b</sup>Max Planck Institute for the Structure and Dynamics of Matter, Luruper Chaussee 149, 22761, Hamburg, Germany

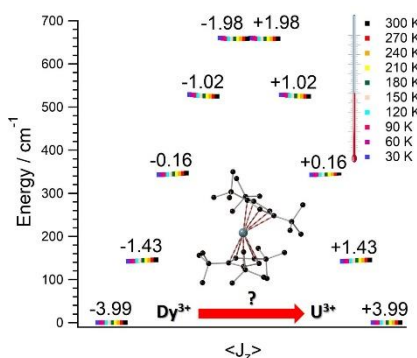
## **Corresponding Author**

\*E-mail: jose.baldovi@mpsd.mpg.de

ABSTRACT. One of the main roadblocks that still hampers the practical use of molecular magnets is their cryogenic working temperature. In the pursuit of rational strategies to design new nanomagnets with increasing blocking temperature, *ab initio* methodologies play an important role by guiding synthetic efforts in the labs. Nevertheless, these methodologies are still too computationally demanding to provide a useful predictive framework. Herein, we present an inexpensive first-principles method devoted to evaluate magnetic relaxation in f-block-based molecular magnets, where only one CASSCF calculation is required. We propose a case study to

illustrate the method and propose chemical modifications in the ligand environment that may help to suppress magnetic relaxation.

## TOC GRAPHICS



**KEYWORDS** Coordination Chemistry, Molecular Magnetism, Single-Ion Magnet, Molecular Magnetic Relaxation, Molecular Vibrations, Computational Chemistry.

Molecular Magnetism is a well-established research field nurtured by a plethora of scientific disciplines. Among several applications,<sup>1,2</sup> molecular magnets are potential candidates for classical information storage, and are raising an unprecedented interest because of recent groundbreaking results.<sup>3-5</sup> A set of key parameters characterize the performance of a molecular magnet. Among them, blocking temperature and magnetic relaxation time are two of the most important ones. Raising these figures of merit in new systems is a main goal, either to understand magnetic relaxation for fundamental reasons, or to develop operative magnets as a practical purpose.

The target features that have commonly been addressed to block relaxation are (i) the electron spin magnitude, and (ii) the potential barrier that separates the ground doublet components.<sup>6</sup> Indeed, the search for new nanomagnets by increasing (i) and (ii) is consistent with an Orbach-like relaxation mechanism, which involves a step-by-step transit of the spin population across the potential barrier. While this strategy has worked for so long and has provided general synthetic rules,<sup>7,8</sup> the recent interest in molecular magnets operating at increasing temperatures makes this picture be insufficient.<sup>6</sup> To gain deeper control on demagnetization, spin-vibration coupling must be incorporated, which dominates relaxation at high temperatures.

The current pursuit of predictive power is encouraging the development of fully *ab initio* approximations.<sup>9,10</sup> Nevertheless, first-principles evaluations of spin-vibration coupling are known to be computationally demanding, since many expensive CASSCF calculations are required.<sup>3,9</sup> Thus, searching for new methodologies able to circumvent this computational bottleneck is of paramount urgency. In the case of lanthanide-based nanomagnets, there already exist affordable semi-empirical approximations based on effective models,<sup>11,12</sup> whose performance can become comparable to that of *ab initio* calculations.<sup>13,14</sup>

Herein, we present an inexpensive first-principles method to estimate effective demagnetization barriers  $U_{eff}$ , relaxation pathways and relaxation rates  $\tau^{-1}$  at any temperature in lanthanide and uranium based molecular nanomagnets. Crystal field parameters (CFPs) are determined by millisecond calculations and only one CASSCF evaluation is required. The method identifies those vibrations promoting relaxation to rationally re-design the given molecule, and incorporates for the first time a temperature dependence in the spin-vibration coupling matrix elements. Contributions from spin-spin dipole coupling to  $U_{eff}$  and  $\tau^{-1}$  can be incorporated by

resorting to recent first-principles proposals.<sup>15</sup> Since the potential barrier may increase from lanthanides to actinides due to a stronger ligand field, and given the challenging computational nature of the  $U^{3+}$  ion,<sup>16,17</sup> we propose to evaluate the effectiveness of bis-metalloocene ligands on actinides and test the efficiency of our method by replacing the  $Dy^{3+}$  ion in  $[Dy(Cp^{III})_2]^+$ , which holds one of the latest records in the blocking temperature,<sup>3</sup> by  $U^{3+}$ .

The method consists of the following three steps: geometry relaxation and vibrational spectrum calculation, determination of CFPs, and evaluation of magnetic relaxation dynamics:

**Step 1.** First, the relevant atom set is relaxed until reaching a minimum in its potential energy surface.<sup>6</sup> This set may be a molecule,<sup>9</sup> or the unit cell of a crystal.<sup>10</sup> We save harmonic frequencies  $\{\nu_j\}_j$ , reduced masses  $\{m_j\}_j$ , and displacement vectors  $\{\overline{w}_j\}_j$  that determine the 3D-direction in which each atom vibrates around its equilibrium position.

**Step 2.** Now, one performs a CASSCF evaluation on the experimental molecular structure to extract the lowest  $2J+1$  energies, where  $J$  is the metal ion ground electron spin quantum number. Then, once the coordinate origin is placed at the metal experimental position, the experimental positions of those metal-coordinating atoms are introduced in the SIMPRE package, see SI.<sup>11,12</sup> This code calculates the CFPs by considering each coordinating atom as an effective point charge, and performs a millisecond diagonalization of the ground  $J$  crystal field Hamiltonian. The charge magnitudes and the metal-charge radial distances are varied to fit the CASSCF energies,<sup>18,19</sup> see SI. Thus, we project the CASSCF information onto the first coordination sphere via effective parameters. Note that the contribution of the coordinating atoms to the ligand field almost recover the whole effect of magnetic anisotropy. Nevertheless, one can include non-coordinating ligand atoms if a significant contribution is expected. To

reduce computational cost, sometimes it is enough to keep the same charge magnitude and radial distance variation in each coordinating atom. This procedure is fully *ab initio*, but one can avoid the CASSCF evaluation and use the experimental energies if they are available. In this case, the experimental structure used in SIMPRE should be determined at the same temperature as that of the experimental energies. Now, the coordinating atom positions in the relaxed geometry are radially varied with the same fitting distance variations determined by SIMPRE. By using the same found charge values, we calculate the equilibrium CFPs  $\left\{ \left( A_k^q \langle r^k \rangle \right)_{eq} \right\}_{k,q}$  in Stevens notation. Unlike lanthanides, excited  $J$  multiplets may have a sizeable weight in the low-lying electronic structure of actinide nanomagnets. Thus, in case of  $U^{3+}$ , to determine the charge magnitude and the radial distance variation, the energy fitting must be replaced by a fitting of the SIMPRE CFPs to the CFPs either CASSCF or experimental.

The diagonalization of the equilibrium crystal field Hamiltonian  $\hat{H}_{eq} = \sum_{k=2,4,6} \sum_{q=-k}^k \left( A_k^q \langle r^k \rangle \right)_{eq} \eta_k \hat{O}_k^q$  in SIMPRE provides the lowest  $2J + 1$  equilibrium eigenstates  $|i\rangle, |f\rangle$  and energies  $E_i, E_f$ , see SI. For  $U^{3+}$ , the diagonalization is performed with the CONDON package,<sup>20</sup> which contains the excited  $J$  multiplets and the CFPs must be introduced in Wybourne notation. The obtained eigenstates are truncated to the ground  $J$  ordered basis set  $\{|-J\rangle, \dots, |+J\rangle\}$  and then renormalized.

The perturbing Hamiltonians  $\left\{ \hat{H}_j = \sum_{k=2,4,6} \sum_{q=-k}^k \Delta \left( A_k^q \langle r^k \rangle \right)_j (T) \eta_k \hat{O}_k^q \right\}_j$ , which are also built with the above ordered basis set, account for the perturbation to the equilibrium electronic structure

from each mode  $j$ , see SI. Their determination requires to estimate the change  $\Delta\left(A_k^q\langle r^k\rangle\right)_j(T)$  produced in  $\left(A_k^q\langle r^k\rangle\right)_{eq}$  after activating each mode  $j$ . We use a model derived by us elsewhere,<sup>9</sup> which provides the following perturbative expression up to second-order in mode coordinate  $Q_j$ :

$$\Delta\left(A_k^q\langle r^k\rangle\right)_j(T) = \frac{\hbar}{4\pi} \left( \frac{\partial^2 A_k^q \langle r^k \rangle}{\partial Q_j^2} \right)_{eq} \frac{1}{m_j \nu_j} \left( \langle n_j \rangle + \frac{1}{2} \right) \quad \text{Eq. 1}$$

Thus, each  $\hat{H}_j$  allows determining the spin-vibration coupling matrix element  $\langle i | \hat{H}_j | f \rangle$ , see SI. The temperature dependence is introduced for the first time in these matrix elements through each boson number  $\langle n_j \rangle = 1 / \left( e^{\hbar \nu_j / k_B T} - 1 \right)$ .

The calculation of the second derivatives  $\left( \partial^2 A_k^q \langle r^k \rangle / \partial Q_j^2 \right)_{eq}$ , evaluated at the relaxed geometry, is as follows. For each mode  $j$ , several distorted geometries  $\left\{ \overrightarrow{v}_d^j \right\}_d$  are generated around the relaxed geometry  $\overrightarrow{v}_{eq}$  by following the corresponding displacement vector  $\overrightarrow{w}_j$ , see SI. Now, we calculate the CFPs at each  $\overrightarrow{v}_d^j$  by following the same procedure to determine  $\left\{ \left( A_k^q \langle r^k \rangle \right)_{eq} \right\}_{k,q}$ . Namely, to apply the same radial distance variations and charge magnitudes to the metal-coordinating atoms in these distorted geometries. Thus, for each mode  $j$  and each CFP we have a set of pairs  $\left\{ \left( \left( A_k^q \langle r^k \rangle \right)_j^d, Q_j^d \right) \right\}_d$ . By fitting the representation “ $\left( A_k^q \langle r^k \rangle \right)_j^d$  vs  $Q_j^d$ ” to a polynomial and evaluating its second derivative at  $Q_j = 0$  we access  $\left( \partial^2 A_k^q \langle r^k \rangle / \partial Q_j^2 \right)_{eq}$ , see SI.

**Step 3.** This step is undertaken by solving the master equation, Eq. 2,<sup>3,21,22</sup> which describes the time evolution of a molecular spin subject to a double-well anisotropy composed of the lowest  $2J+1$  equilibrium eigenstates. The energy that induces the spin to relax comes from the interaction with surrounding vibrations. Intuitively, at each time  $t$  there is a probability  $p_i(t)$  of being in an eigenstate  $|i\rangle$ . At a time  $t+dt$  the system may make a transition to a different eigenstate  $|f\rangle$  with a probability  $\gamma_{if}dt$ , either by absorbing or by emitting a phonon. The net difference between the input  $\gamma_{fi}p_i$  and output  $\gamma_{if}p_f$  spin population flows equals the change in time of  $p_i$ . Thus, once the transitions are assumed to be independent, these probabilities evolve as:

$$\frac{dp_i(t)}{dt} = \sum_{f=1, f \neq i}^{2J+1} [\gamma_{if}p_f(t) - \gamma_{fi}p_i(t)], \quad i=1, \dots, 2J+1 \quad \text{Eq. 2}$$

The transition rates  $\gamma_{if}$  and  $\gamma_{fi}$  account for the spin population flow between  $|i\rangle$  and  $|f\rangle$ , and their expressions depend on the relaxation process to model. We include two important processes: (i) Orbach and (ii) second-order Raman. To get further insight, the most likely relaxation pathway can also be determined. Then, those vibrations promoting each relaxation step are identified and modifications on the molecular structure can be proposed to suppress demagnetization. All details are routine and found in SI.<sup>3,21-23</sup> The same procedure applies if the crystal field Hamiltonians are expanded to include a static magnetic field via a Zeeman term. We provide home-made codes in SI to carry out these steps.

**A case study:**  $[\text{U}(\text{Cp}^{\text{t}})_2]^+$ . Because of the larger size of  $\text{U}^{3+}$  compared to  $\text{Dy}^{3+}$ , we propose to use a counter-ion different from  $[\text{B}(\text{C}_6\text{F}_5)_4]^-$  with bulkier substituents in the synthetic process, as

$F^-$  could coordinate the  $U^{3+}$  ion. Since we lack a  $[U(Cp^{III})_2]^+$  structure, we use the experimental geometry of  $[Dy(Cp^{III})_2]^+$ .<sup>3</sup> By replacing  $Dy^{3+}$  by  $U^{3+}$ , we carry out the geometry relaxation and the vibrational spectrum calculation, see Fig.1 and SI. As explained, we should first perform a CASSCF evaluation on a real structure of  $[U(Cp^{III})_2]^+$  to obtain the equilibrium CFPs set  $\left\{ \left( A_k^q \langle r^k \rangle \right)_{eq} \right\}_{k,q}$ . Since this is not possible, we proceed as explained in SI to determine the equilibrium electronic structure, see Fig. 1.

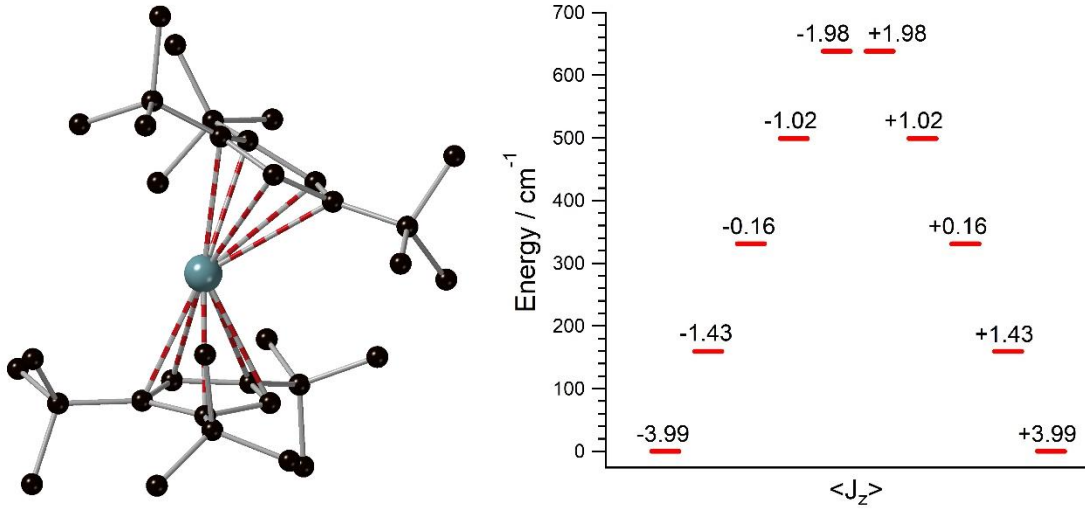


**Figure 1.** Left: Equilibrium geometry of  $[U(Cp^{III})_2]^+$ . Hydrogen atoms omitted for clarity. Right:  $[U(Cp^{III})_2]^+$  lowest  $2J+1$  equilibrium energies. The numbers above each level are the  $J_z$  expectation values of the equilibrium eigenstates after being truncated to the  $|m_J\rangle$  components of the  $U^{3+}$  ground electron spin quantum number  $J = 9/2$  and then renormalized.

Once the  $\left( A_k^q \langle r^k \rangle \right)_{eq}$  and  $\left( \partial^2 A_k^q \langle r^k \rangle / \partial Q_j^2 \right)_{eq}$  parameters are determined, we calculate the CFPs thermal evolution.<sup>9</sup> From Fig. 2, important contributions from off-diagonal CFPs are clearly observed, which leads to a sizeable  $|m_J\rangle$  mixing in the equilibrium eigenstates, see SI. This fact

opposes a good single-molecule magnet behavior, where the diagonal CFPs should largely dominate over the off-diagonal ones. Another feature is the small yet significant relative change in some CFPs. A proper tuning in the chemical structure aimed to reduce the variations  $\Delta\left(A_k^q \langle r^k \rangle\right)_j$  would improve the molecular magnet performance.<sup>9</sup> Indeed, this reduction would make the matrix elements  $\langle i | \hat{H}_j | f \rangle$  and the transition rates  $\gamma$  be smaller, since the perturbing Hamiltonians  $\hat{H}_j$  are proportional to  $\Delta\left(A_k^q \langle r^k \rangle\right)_j$ .

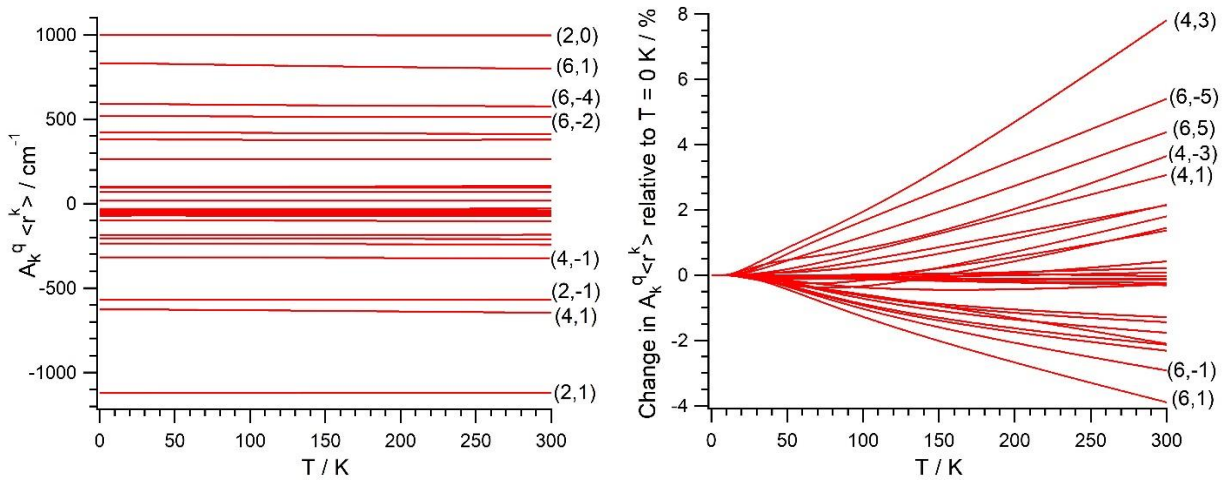


**Figure 2.** Absolute (left) and relative to  $T = 0$  K (right) thermal evolution of the CFPs. Some parameters are identified as  $(k,q)$ , where  $k$  and  $q$  are the scripts  $k = 2, 4, 6$  and  $q = -k, \dots, +k$ .

Fig. 3 shows the thermal dependence of relaxation time  $\tau$  when Orbach transitions rates are used in Eq. 2. Above 30 K the thermally-activated regime is at play. As seen in the relaxation pathway at 30 K in Fig. 4, the 50% of the initial population in the  $\langle J_z \rangle = -3.99$  eigenstate is promoted to the  $\langle J_z \rangle = -1.43$  eigenstate in the first excited doublet, while the remaining 50% tunnels the barrier and reaches the  $\langle J_z \rangle = +1.43$  eigenstate. From the  $\langle J_z \rangle = -1.43$  eigenstate,

the 25% of the population is promoted to the second excited doublet, which subsequently transits to the  $\langle J_z \rangle = +1.43$  eigenstate before decaying to the ground  $\langle J_z \rangle = +3.99$  eigenstate. As temperature is increased there exist more available phonons. At 50 K the 48% of population in the  $\langle J_z \rangle = -1.43$  eigenstate is now promoted to the second excited doublet, while only the 1.7% tunnels the barrier and reaches the ground  $\langle J_z \rangle = +3.99$  eigenstate. Among the calculated vibrations, six of them are clearly responsible for the transition rates involved in these relaxation pathways, see animations. In SI we propose several structural modifications for  $[\text{U}(\text{Cp}^{\text{ttt}})_2]^+$  in order to remove these molecular vibrations and partially block the Orbach-driven magnetic relaxation. In this thermally-activated regime, the estimated Orbach prefactor,  $\tau_0 = e^{-17.43} = 2.7 \cdot 10^{-8}$  s, is inside of the commonly observed  $10^{-5} - 10^{-10}$  s range.<sup>24</sup> The effective demagnetization barrier  $U_{\text{eff}} = 292$  K is in the hundreds of kelvin, something typical in a large set of recent molecular magnets,<sup>24</sup> and is found around  $40 \text{ cm}^{-1}$  above the first excited doublet.

Below 30 K, little or rather negligible spin population is promoted to the second excited doublet, which mostly tunnels the barrier through the first excited doublet. Nevertheless, the calculated Orbach-based relaxation times are now much larger than those found in most of molecular magnets. Thus, a different mechanism could be dominating magnetic relaxation such as quantum tunneling between the ground doublet components, which is not recovered by our approach but is commonly observed at these low temperatures.<sup>4,5</sup>

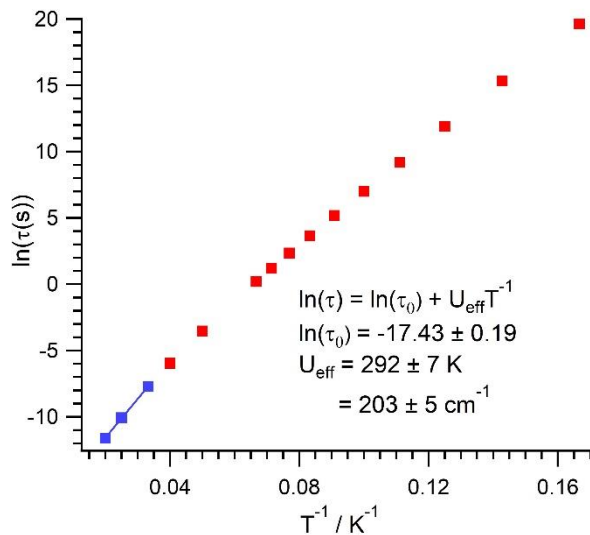


**Figure 3.** Thermal evolution of relaxation time  $\tau$  calculated from the Orbach transition rates, along with fit to determine both the Orbach prefactor  $\tau_0$  and the effective demagnetization barrier  $U_{\text{eff}}$  in the thermally-activated regime ( $T \geq 30\text{K}$ ).

We have also evaluated Eq. 2 by employing the second-order Raman transition rates. The corresponding thermal evolution of relaxation time  $\tau$  is found in Table S1. These Raman-based  $\tau$  values are five orders of magnitude larger than those calculated with the Orbach transition rates, see Fig. 3. Thus, second-order Raman process should be discarded as a competitive mechanism in a real experiment, such as it was found in  $[\text{Dy}(\text{Cp}^{\text{ttt}})_2]^+$ .<sup>3</sup>

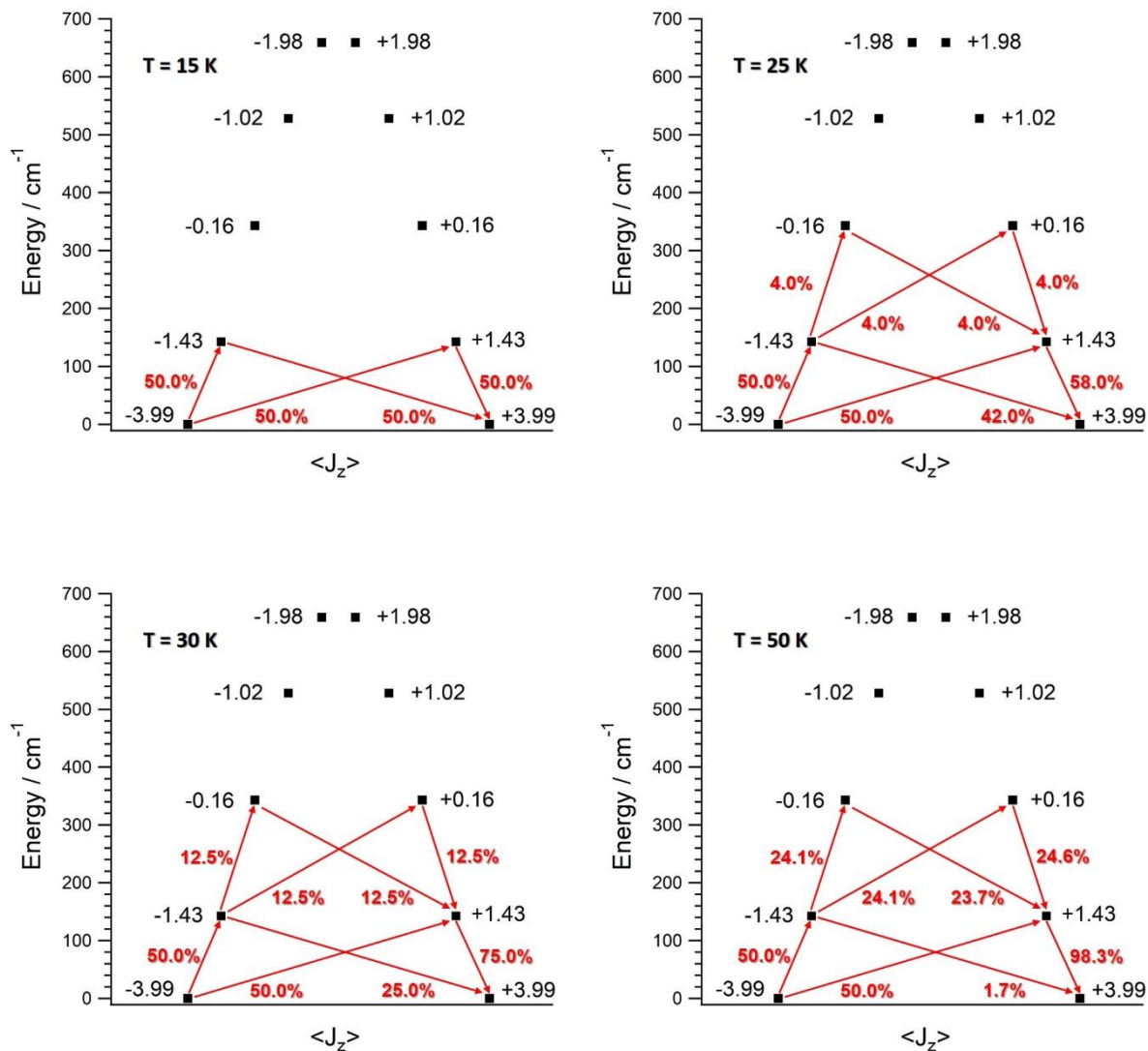


**Figure 4.** Orbach-driven relaxation pathways for different temperatures starting at the  $\langle J_z \rangle = -3.99$  eigenstate with unity population. The outcome population sum from a given eigenstate equals the income population sum to the same eigenstate. Populations lesser than 1.0% are not shown.

Even though the use of bis-metalloccenium ligands, our calculated  $[\text{U}(\text{Cp}^{\text{ttt}})_2]^+$  effective demagnetization barrier ( $\sim 292\text{K}$ ) is one order of magnitude below those reported for  $[\text{Dy}(\text{Cp}^{\text{ttt}})_2]^+$  ( $\sim 1760\text{K}$ ),<sup>3</sup> and  $\text{Dy-5}^*$  ( $\sim 2217\text{K}$ ).<sup>5</sup> Besides, the maximum temperature in

$[\text{U}(\text{Cp}^{\text{III}})_2]^+$  ( $\sim 50\text{K}$ ) at which the experimental relaxation time is still above the standard experimental detection limit is also clearly smaller as compared to  $[\text{Dy}(\text{Cp}^{\text{III}})_2]^+$  ( $\sim 112\text{K}$ ),<sup>3</sup> and Dy-5\* ( $\sim 138\text{K}$ ).<sup>5</sup> Nonetheless, the calculated  $[\text{U}(\text{Cp}^{\text{III}})_2]^+$  Orbach prefactor  $\tau_0 \sim 2.7 \cdot 10^{-8}\text{s}$  is at least three orders of magnitude above the ones corresponding to these two Dy-based molecular magnets ( $\tau_0 \sim 2.0 \cdot 10^{-11}\text{s}$  and  $\tau_0 \sim 4.2 \cdot 10^{-12}\text{s}$ , resp.).<sup>3,5</sup> This Orbach prefactor is among the smallest ones that have been experimentally determined in uranium molecular magnets.<sup>16,17</sup> On the other hand, there do exist two significant advances respect to previous uranium nanomagnets: (i) the standard effective barrier was in the range of dozens of kelvin, and now  $[\text{U}(\text{Cp}^{\text{III}})_2]^+$  reaches several hundreds of kelvin ( $\sim 292\text{K}$ ),<sup>16,17</sup> (ii) by assuming that the thermally-activated regime (Orbach process) dominates between 30 K – 50 K in  $[\text{U}(\text{Cp}^{\text{III}})_2]^+$ , see Figs. 3 and 4, while so far it was not possible to determine relaxation times beyond 5 K,<sup>16,17</sup> the experimental detection limit  $\tau \sim 10^{-6}\text{s}$  in case of  $[\text{U}(\text{Cp}^{\text{III}})_2]^+$  would be now found at 50 K. Thus, it seems clear that  $[\text{U}(\text{Cp}^{\text{III}})_2]^+$  is not expected to outperform the recent highly-performing  $[\text{Dy}(\text{Cp}^{\text{III}})_2]^+$  and Dy-5\* magnets. Yet, it may be representative of an important step forward in the design of uranium-based magnets.

In this manuscript we have proposed a novel first-principles methodology devoted to shed light on the magnetic relaxation of f-block molecular magnets. Three main steps are involved: (1) geometry relaxation and vibrational mode calculation, (2) determination of CFPs, (3) evaluation of spin dynamics. The method offers the important advantage of significantly reducing the computational cost while keeping the calculation accuracy inside an acceptable range. Indeed, all but one of the expensive CASSCF calculations required in previous methods are now replaced by millisecond calculations. Besides, our approach introduces for the first time a temperature dependence in the spin-vibration coupling matrix elements. To demonstrate this methodology,

we consider the outstanding molecular magnet  $[\text{Dy}(\text{Cp}^{\text{III}})_2]^+$  and find that the replacement of  $\text{Dy}^{3+}$  by  $\text{U}^{3+}$  does not result in an enhanced performance. Yet,  $[\text{U}(\text{Cp}^{\text{III}})_2]^+$  does outperform all previously reported uranium-based nanomagnets. One of the critical factors that help to promote relaxation in  $[\text{U}(\text{Cp}^{\text{III}})_2]^+$  may be the noticeable mixing among the  $|m_j\rangle$  components in the equilibrium eigenstates of the ground  $J$  multiplet. Importantly, this mixing is also found in previously reported uranium molecular magnets,<sup>16,17,25</sup> but not in the cutting-edge Dy-based magnets  $[\text{Dy}(\text{Cp}^{\text{III}})_2]^+$  and Dy-5\* even though the ligand coordination is not strictly axial.<sup>3,5</sup> Our analysis shows that there exist similar molecular vibrations promoting relaxation in  $[\text{Dy}(\text{Cp}^{\text{III}})_2]^+$ , Dy-5\* and  $[\text{U}(\text{Cp}^{\text{III}})_2]^+$ , see SI. Rocking-like deformations of the  $\text{Cp}^{\text{III}}$  rings where directly bounded hydrogen atoms move towards and away from the metal ion are present both in  $[\text{Dy}(\text{Cp}^{\text{III}})_2]^+$  and in  $[\text{U}(\text{Cp}^{\text{III}})_2]^+$ . On the other hand, out-of-plane ring vibrations are also found both in Dy-5\* and in  $[\text{U}(\text{Cp}^{\text{III}})_2]^+$ . Those vibrations in  $[\text{U}(\text{Cp}^{\text{III}})_2]^+$  that are common to  $[\text{Dy}(\text{Cp}^{\text{III}})_2]^+$  and Dy-5\* could be blocked by placing bulkier substituents in the coordinating rings than hydrogen atoms (this was already done in ref. 5 and worked: both the blocking temperature and the effective barrier are increased respect to ref. 3), and by bounding the two coordinating rings such as in stapled bis-phthalocyanines. In fact, the frequencies of the six vibrations that promote thermally-activated relaxation in  $[\text{U}(\text{Cp}^{\text{III}})_2]^+$  closely match the gaps between the equilibrium ground and first excited doublets ( $159.3\text{ cm}^{-1}$ ), and first and second excited doublets ( $171.7\text{ cm}^{-1}$ ) in Fig. 1, see SI. Thus, the molecular magnet performance would also benefit from any structural modification that takes the frequencies of these vibrations out of resonance with the given energy gaps. Hence, we conclude that there may be still room for further improvement in the employed bis-metallocenium ligands.

ASSOCIATED CONTENT

**Supporting Information.** The following files are available free of charge.

Supplementary information (file escalera-baldovi-coronado-SI). Input and outputs of the geometry relaxation and the vibrational spectrum calculation (subfolder Relax-Geom-Vib-Spec-Calc). CFPs evolution against distortion coordinates (subfolder CFPs-vs-Dist-Coord). Fortran codes, inputs and outputs to evaluate magnetic relaxation dynamics and to calculate CFPs thermal evolutions (Home-Made-Codes). Orbach-driven magnetization decays with time (subfolder Orbach-mag). Master matrices and diagonalization, relaxation pathways and vibrational mode contributions (subfolder Orbach-rp-Raman). Animations of the  $[\text{U}(\text{Cp}^{\text{ttt}})_2]^+$  calculated vibrational modes (subfolder Animations).

#### AUTHOR INFORMATION

##### Notes

The authors declare no competing financial interests.

#### ACKNOWLEDGMENT

The present work has been funded by the EU (COST Action CA15128 MOLSPIN, ERC-2014-CoG-647301 DECRESIM, ERC-2018-AdG-788222 MOL-2D), the Spanish MINECO (Unit of excellence “María de Maeztu” MDM-2015-0538 and grants MAT2017-89993-R, CTQ2017-89528-P) and the Generalitat Valenciana (Prometeo Program of excellence).

#### REFERENCES

- (1) Gaita-Ariño, A.; Luis, F.; Hill, S.; Coronado, E. Molecular Spins for Quantum Technologies. *Nat. Chem.* **2019**, 11, 301-309.

- (2) Guo, L.; Gu, X.; Zhu, X.; Sun, X. Recent Advances in Molecular Spintronics: Multifunctional Spintronic Devices. *Adv. Mater.* **2019**, <https://doi.org/10.1002/adma.201805355>
- (3) Goodwin, C. A. P.; Ortu, F.; Reta, D.; Chilton, N. F.; Mills, D. P. Molecular Magnetic Hysteresis at 60 Kelvin in Dysprosocenium. *Nature* **2017**, 548, 439-442.
- (4) McClain, K. R.; Gould, C. A.; Chakarawet, K.; Teat, S. J.; Groshens, T. J.; Long, J. R.; Harvey, B. G. High-Temperature Magnetic Blocking and Magneto-Structural Correlations in a Series of Dysprosium(III) Metallocenium Single-Molecule Magnets. *Chem. Sci.* **2018**, 9, 8492-8503.
- (5) Guo, F.-S.; Day, B. M.; Chen, Y.-C.; Tong, M.-L.; Mansikkamäki, A.; Layfield, R. A. Magnetic Hysteresis up to 80 Kelvin in a Dysprosium Metallocene Single-Molecule Magnet. *Science* **2018**, 362(6421), 1400-1403.
- (6) Escalera-Moreno, L.; Baldoví, J. J.; Gaita-Ariño, A.; Coronado, E. Spin States, Vibrations and Spin Relaxation in Molecular Nanomagnets and Spin Qubits: A Critical Perspective. *Chem. Sci.* **2018**, 9, 3265-3275.
- (7) Baldoví, J. J.; Cardona-Serra, S.; Clemente-Juan, J. M.; Coronado, E.; Gaita-Ariño, A.; Palií, A. Rational Design of Single-Ion Magnets and Spin Qubits Based on Mononuclear Lanthanoid Complexes. *Inorg. Chem.* **2012**, 51(22), 12565-12574.
- (8) Rinehart, J. D.; Long, J. R. Exploiting Single-Ion Anisotropy in the Design of f-Element Single-Molecule Magnets. *Chem. Sci.* **2011**, 2, 2078-2085.
- (9) Escalera-Moreno, L.; Suaud, N.; Gaita-Ariño, A.; Coronado, E. Determining Key Local Vibrations in the Relaxation of Molecular Spin Qubits and Single-Molecule Magnets. *J. Phys. Chem. Lett.* **2017**, 8(7), 1695-1700.
- (10) Lunghi, A.; Totti, F.; Sessoli, R.; Sanvito, S. The Role of Anharmonic Phonons in Under-Barrier Spin Relaxation of Single Molecule Magnets. *Nat. Commun.* **2017**, 8, 14620.

- (11) Baldoví, J. J.; Clemente-Juan, J. M.; Coronado, E.; Gaita-Ariño, A.; Palić, A. An Updated Version of the Computational Package SIMPRE that uses the Standard Conventions for Stevens Crystal Field Parameters. *J. Comput. Chem.* **2014**, 35(26), 1930-1934.
- (12) Cardona-Serra, S.; Escalera-Moreno, L.; Baldoví, J. J.; Gaita-Ariño, A.; Clemente-Juan, J. M.; Coronado, E. SIMPRE1.2: Considering the Hyperfine and Quadrupolar Couplings and the Nuclear Spin Bath Decoherence. *J. Comput. Chem.* **2016**, 37(13), 1238-1244.
- (13) Hallmen, P. P.; Köppl, C.; Rauhut, G.; Stoll, H.; van Slageren, J. Fast and Reliable Ab Initio Calculation of Crystal Field Splittings in Lanthanide Complexes. *J. Chem. Phys.* **2017**, 147, 164101.
- (14) Calvello, S.; Piccardo, M.; Rao, S. V.; Soncini, A. CERES: An Ab Initio Code dedicated to the Calculation of the Electronic Structure and Magnetic Properties of Lanthanide Complexes. *J. Comput. Chem.* **2017**, 39(6), 328-337.
- (15) Aravena, D. Ab Initio Prediction of Tunneling Relaxation Times and Effective Demagnetization Barriers in Kramers Lanthanide Single-Molecule Magnets. *J. Phys. Chem. Lett.* **2018**, 9, 5327-5333.
- (16) Coutinho, J. T.; Perfetti, M.; Baldoví, J. J.; Antunes, M. A.; Hallmen, P. P.; Bamberger, H.; Crassee, I.; Orlita, M.; Almeida, M.; van Slageren, J.; Pereira, L. C. J. Spectroscopic Determination of the Electronic Structure of a Uranium Single-Ion Magnet. *Chem. Eur. J.* **2019**, 25(7), 1758-1766.
- (17) Baldoví, J. J.; Cardona-Serra, S.; Clemente-Juan, J. M.; Coronado, E.; Gaita-Ariño, A. Modeling the Properties of Uranium-based Single Ion Magnets. *Chem. Sci.* **2013**, 4, 938-946.
- (18) Baldoví, J. J.; Borrás-Almenar, J. J.; Clemente-Juan, J. M.; Coronado, E.; Gaita-Ariño, A. Modeling the Properties of Lanthanoid Single-Ion Magnets using an Effective Point-Charge Approach. *Dalton. Trans.* **2012**, 41, 13705-13710.

- (19) Baldoví, J. J.; Gaita-Ariño, A.; Coronado, E. Modeling the Magnetic Properties of Lanthanide Complexes: Relationship of the REC Parameters with Pauling Electronegativity and Coordination Number. *Dalton. Trans.* **2015**, 44, 12535-12538.
- (20) van Leusen, J.; Speldrich, M.; Schilder, H.; Kögerler, P. Comprehensive Insight into Molecular Magnetism via CONDON: Full vs. Effective Models. *Coord. Chem. Rev.* **2015**, 289-290, 137-148.
- (21) Gatteschi, D.; Sessoli, R.; Villain, J. *Molecular Nanomagnets*. **2006**, Oxford, University Press.
- (22) Alexander, M. H.; Hall, G. E.; Dagdigian, P. J. The Approach to Equilibrium: Detailed Balance and the Master Equation. *J. Chem. Educ.* **2011**, 88(11), 1538-1543.
- (23) Orbach, R. Spin-Lattice Relaxation in Rare-Earth Salts. *Proc. Roy. Soc. A.* **1961**, 264, 458-484.
- (24) Yang J.-W.; Tian, Y.-M.; Tao, J.; Chen, P.; Li, H.-F; Zhang, Y.-Q.; Yan, P. F.; Sun, W.-B. Modulation of the Coordination Environment around the Magnetic Easy Axis Leads to Significant Magnetic Relaxations in a Series of 3d-4f Schiff Complexes. *Inorg. Chem.* **2018**, 57, 8065-8077.
- (25) Antunes, M. A.; Coutinho, J. T.; Santos, I. C.; Marçalo, J.; Almeida, M.; Baldoví, J. J.; Pereira, L. C. J.; Gaita-Ariño, A.; Coronado, E. A Mononuclear Uranium(IV) Single-Molecule Magnet with an Azobenzene Radical Ligand. *Chem. Eur. J.* **2015**, 21(49), 17817-17826.